Progressing Toward a Cohesive Pediatric ^{18}F-FDG PET/MR Protocol: Is Administration of Gadolinium Chelates Necessary?

Christopher Klenk[1], Rakhee Gawande[1], Vy Thao Tran[1], Jennifer Trinh Leung[1], Kevin Chi[1], Daniel Owen[1], Sandra Luna-Fineman[2], Kathleen M. Sakamoto[2], Alex McMillan[1], Andy Quon[1], and Heike E. Daldrup-Link[1]

[1]Department of Radiology, Molecular Imaging Program at Stanford, and Lucile Packard Children's Hospital, Stanford University, Stanford, California; and [2]Department of Pediatrics, Lucile Packard Children's Hospital, Stanford University, Stanford, California

With the increasing availability of integrated PET/MR scanners, the utility and need for MR contrast agents for combined scans is questioned. The purpose of our study was to evaluate whether administration of gadolinium chelates is necessary for evaluation of pediatric tumors on ^{18}F-FDG PET/MR images. **Methods:** First, in 119 pediatric patients with primary and secondary tumors, we used 14 diagnostic criteria to compare the accuracy of several MR sequences: unenhanced T2-weighted fast spin-echo imaging; unenhanced diffusion-weighted imaging; and—before and after gadolinium chelate contrast enhancement—T1-weighted 3-dimensional spoiled gradient echo LAVA (liver acquisition with volume acquisition) imaging. Next, in a subset of 36 patients who had undergone ^{18}F-FDG PET within 3 wk of MRI, we fused the PET images with the unenhanced T2-weighted MR images (unenhanced ^{18}F-FDG PET/MRI) and the enhanced T1-weighted MR images (enhanced ^{18}F-FDG PET/MRI). Using the McNemar test, we compared the accuracy of the two types of fused images using the 14 diagnostic criteria. We also evaluated the concordance between ^{18}F-FDG avidity and gadolinium chelate enhancement. The standard of reference was histopathologic results, surgical notes, and follow-up imaging. **Results:** There was no significant difference in diagnostic accuracy between the unenhanced and enhanced MR images. Accordingly, there was no significant difference in diagnostic accuracy between the unenhanced and enhanced ^{18}F-FDG PET/MR images. ^{18}F-FDG avidity and gadolinium chelate enhancement were concordant in 30 of the 36 patients and 106 of their 123 tumors. **Conclusion:** Gadolinium chelate administration is not necessary for accurate diagnostic characterization of most solid pediatric malignancies on ^{18}F-FDG PET/MR images, with the possible exception of focal liver lesions.

Key Words: PET/MR; PET-MR fusion; pediatric oncology; MR contrast utility; ^{18}FDG-PET

J Nucl Med 2016; 57:70–77
DOI: 10.2967/jnumed.115.161646

MRI is becoming the modality of choice for local staging of malignancies in pediatric patients, including neurogenic tumors (*1*), Wilms tumor (*2*), hepatoblastoma (*3*), hepatocellular carcinoma (*4*), and germ cell tumors and sarcomas (*5*), among others (*6*). For some of these tumors, such as sarcomas and lymphomas, ^{18}F-FDG PET/CT is added for whole-body staging (*7*). Novel integrated ^{18}F-FDG PET/MR scanners significantly reduce radiation exposure compared with ^{18}F-FDG PET/CT scanners. Combining local and whole-body staging into a single PET/MR session would enable 1-stop-shop tumor staging and avoid repeated anesthesia in small children. However, each MR scan for local and whole-body staging takes close to an hour (*8*). Economical and practical considerations mandate a streamlined protocol for local and whole-body scans such that the combined examination could be done in about an hour or less. The initial ^{18}F-FDG PET/MR studies of abdominal and pelvic tumors in adults were performed by integrating ^{18}F-FDG PET data with T2-weighted MR images, in-phase gradient echo MR images, or gadolinium chelate–enhanced T1-weighted MR images (*9*). To the best of our knowledge, only a single ^{18}F-FDG PET/MR study of pediatric cancer has integrated ^{18}F-FDG PET data with water-sensitive fast inversion recovery MR images (*10*), and nobody has systematically investigated whether enhancement with gadolinium chelate adds any information to unenhanced ^{18}F-FDG PET/MR images generated either on an integrated system or with software coregistration. The purpose of this study was to determine whether the administration of gadolinium chelate is necessary for local staging of pediatric tumors on MR images or ^{18}F-FDG PET/MR images. If gadolinium chelate administration does not provide additional information, MR images for local staging can be streamlined and gadolinium chelates can be replaced by more specific MR contrast agents (*11,12*).

MATERIALS AND METHODS

Patients

The review board at our institution approved this single-center retrospective study, and the requirement for informed consent was waived. To be included, the patients had to be 0–25 y old, with benign and malignant tumors, contrast-enhanced MRI between 2005 and 2013, and follow-up imaging for at least 12 mo. We included both benign and malignant lesions in order to consider all possible findings in a clinical setting. Exclusion criteria were loss to follow-up and technically inadequate images (e.g., motion artifacts or study not completed). We identified 119 patients who met our inclusion criteria: 66 male and 53 female patients with a mean age of 8.1 (±6.1) years. Of these, 103 patients had primary tumors, 8 patients had multiple liver metastases, 13 patients had multiple bone metastases, and 19 patients had lymph node metastases. The diagnoses of the 119 patients as proven by histopathologic examination and follow-up imaging are listed in Table 1.

Received Jun. 2, 2015; revision accepted Sep. 10, 2015.
For correspondence or reprints contact: Heike E. Daldrup-Link, Department of Radiology, Molecular Imaging Program at Stanford, Stanford School of Medicine, 725 Welch Rd., Room 1665, Stanford, CA 94305.
E-mail: h.e.daldrup-link@stanford.edu
Published online Oct. 15, 2015.

We then selected a subgroup of 36 patients who had also undergone ^{18}F-FDG PET within 3 wk of the MRI and had not received interval treatment between PET and MRI. This subgroup included 14 male and 22 female patients, with an age range of 1–24 y and a mean age of 9.9 y. These patients had 123 tumors as proven by histopathologic examination and follow-up imaging (Table 1).

Imaging Protocols

MRI. Axial MR images of the abdomen or pelvis were obtained on a clinical 1.5-T (Signa HDxt; GE Healthcare) or 3-T (Discovery MR750; GE Healthcare) scanner using 4 sequences. The first was unenhanced T2-weighted fast spin-echo (FSE) imaging (repetition time, 2,000–11,000 ms at 1.5 T and 6,666–12,500 ms at 3 T; echo time, 67–82 ms; slice thickness, 2–4 mm; field of view, 20–32 cm at both field strengths). The second was unenhanced diffusion-weighted imaging (repetition time/echo time: 5,250–7,500/54–64 ms; b = 0, 500). The third and fourth were T1-weighted 3-dimensional spoiled gradient echo LAVA (liver acquisition with volume acquisition) imaging before and after gadolinium chelate contrast enhancement, respectively (gadobenate dimeglumine, 0.1 mmol/kg intravenously [MultiHance; Bracco Diagnostics]) (repetition time, 3.8–7.2 ms; echo time, 1.9–7.2 ms; slice thickness, 2–5 mm; flip angle, 12°–15°; field of view, 24–36 cm).

^{18}F-FDG PET/CT. ^{18}F-FDG PET/CT was performed on an integrated scanner (Biograph 16 [Siemens Medical Solutions] or Discovery VCT [GE Healthcare]). The patients fasted for at least 6 h beforehand to decrease the physiologic blood glucose level and to reduce the serum insulin level to near baseline. Blood glucose was measured before the ^{18}F-FDG was injected. No premedication with muscle

TABLE 1
Distribution of Benign and Malignant Diseases

Benign	*n*	Malignant	*n*
Liver			
Hemangioma	1	Hepatoblastoma	10
Hemangioendothelioma	4	Hepatocellular carcinoma	1
Focal nodular hyperplasia	8	Hepatic metastases from neuroblastoma	3
Hepatic adenoma	1		
Hepatic regenerative nodule	6		
Hepatic abscess presenting as mass	2		
Kidney			
Mesoblastic nephroma	1	Wilms tumors	9
Renal abscess presenting as mass	2	Renal cell carcinoma	1 (1)
Angiomyolipoma	1		
Adrenal			
Ganglioneuroma	2	Neuroblastoma	9 (3)
		Adrenocortical carcinoma	1
Spleen			
Hemangioma	1		
Lymphangioma	1		
Pancreas			
Pseudopapillary tumor	1	Metastases from neuroblastoma	1
Ovary			
Complex ovarian cyst	1	Granulosa cell tumor	2
Dermoid cyst	1	Germ cell tumor	1 (1)
Teratoma	4 (1)	Papillary ovarian carcinoma	1 (1)
Other lesions			
Aggressive desmoid fibromatosis	3 (1)	Rhabdomyosarcoma	8 (8)
Infradiaphragmatic sequestration presenting as mass	2	Ewing and soft-tissue sarcoma	8 (5)
Schwannoma	2		
Retroperitoneal phlegmon presenting as mass	1	Metastatic lymphadenopathy from neuroblastoma	1
Cystic lymphatic malformation	1	Osteosarcoma	1 (1)
Desmoplastic small round cell tumor	1 (1)	Lymphoma*	13 (12)
		Metastatic sinonasal carcinoma	1
		Nasopharyngeal (nuclear protein in testis) carcinoma	1 (1)

*Including post–renal transplantation lymphoproliferative disorder.
Data in parentheses are proportion of investigated subgroup.

relaxants or sedatives was used. ^{18}F-FDG (7.77 MBq/kg of body weight; 0.14 mCi/kg) was injected intravenously 45–60 min before image acquisition, and the patients were asked to void their urine immediately before the scan. Oral contrast was not administered. Once the patients were positioned in the scanner, Omnipaque 240 or 300 (2.0 mL/kg, the manufacturer's recommended dose for children) was injected intravenously at a rate of 2.0–3.0 mL/s. PET and low-dose diagnostic CT (20–120 mAs) of the whole body were performed in an arms-up position with scanning times of approximately 25–45 min. Emission images were acquired for 3 min per bed position in 3-dimensional mode. The CT data were used for attenuation correction of the PET emission data.

Integration of ^{18}F-FDG PET Images with MR Images. To integrate the anatomic and functional information, we fused the PET images with either the unenhanced T2-weighted MR images (unenhanced ^{18}F-FDG PET/MRI) or the enhanced T1-weighted MR images (enhanced ^{18}F-FDG PET/MRI) using OsiriX software (version 5.6; 64-bit), an open-source DICOM viewer (*13*). It fuses the images by using a transparency mask so that pixels of low signal intensity in the color-shaded ^{18}F-FDG PET image are transparent whereas pixels of high signal intensity are opaque. A radiologist with 5 y of experience manually adjusted image fusion as needed using internal anatomic landmarks such as the outlines of organs, ribs, vertebrae, and pelvic bones.

TABLE 2
Diagnostic Criteria Regarding Morphology, Extent, and Metastases

Parameter	Unenhanced MRI	Enhanced MRI	^{18}F-FDG PET
Morphology			
Solid	Restricted diffusion	Enhancement	Avidity*
Cystic	Hyperintensity on T2 and DWI (T2 shine-through)	No enhancement	No central avidity; exception: single paraspinal abscess
Homogeneous	Uniform T2 and DWI signal	Uniform enhancement	Not applicable
Heterogeneous	Varying T2 and DWI signal	Varying enhancement	Not applicable
Necrosis, areas of decreased/absent enhancement	Heterogeneity/hyperintensity on T2 and DWI (T2 shine-through)	Decreased or absence of enhancement	No avidity, and fluid noted on CT or MRI
Tumor margins	Well-defined = distinct; ill-defined = indistinct	Well-defined = distinct; ill-defined = indistinct	Not applicable since all margins on PET are ill defined
Tumor extent			
Infiltration of adjacent organs	Tumor/avidity extending beyond organ of origin and infiltrating adjacent structures	Tumor/avidity extending beyond organ of origin and infiltrating adjacent structures	Tumor/avidity extending beyond organ of origin and infiltrating adjacent structures
Extension across midline	Tumor/avidity extending beyond margin of contralateral vertebral body	Tumor/avidity extending beyond margin of contralateral vertebral body	Tumor/avidity extending beyond margin of contralateral vertebral body
Encasement of vessels	Tumor/avidity surrounding vessel and extending > 270°; for PET, MRI or CT was used for anatomic correlation	Tumor/avidity surrounding vessel and extending > 270°; for PET, MRI or CT was used for anatomic correlation	Tumor/avidity surrounding vessel and extending > 270°; for PET, MRI or CT was used for anatomic correlation
Tumor thrombosis	Enlarged vein with altered signal on T2 and DWI	Enlarged vein with focus of intraluminal enhancement	Focal linear avidity within vein, either enlarged or contiguous with solid tumor tissue
Metastases			
Solid organ (liver, spleen, kidney, or pancreas)	Hyperintensity on T2 and DWI	Lesion enhancement and washout on delayed images	Avidity obviously greater than background within organ*
Bone marrow	Hyperintensity on T2 and DWI	Tumor enhancement	Avidity, either diffuse or focally within lesion*
Lymph node	Short axis > 1 cm with loss of normal kidney bean shape	Short axis > 1 cm with loss of normal kidney bean shape	Avidity within lymph node despite size*
Final diagnosis	Most appropriate diagnosis based on imaging features	Most appropriate diagnosis based on imaging features	Most appropriate diagnosis based on imaging features

*If equivocal, then region of interest was placed within lesion of concern, and mean SUV_{max} was compared with mediastinal blood pool or hepatic background. Mean $SUV_{max} > 2.5$ was considered suggestive of tumor involvement or metastatic disease.
DWI = diffusion-weighted imaging.

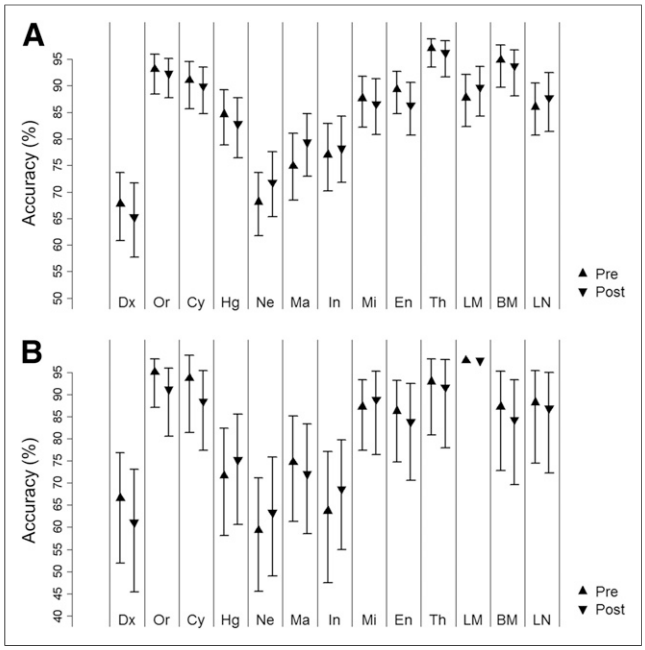

FIGURE 1. Accuracy plots for 13 diagnostic criteria evaluated on unenhanced and enhanced MR images. (A) Data for all 119 patients. (B) Data for the subgroup of 36 patients with ^{18}F-FDG PET/MR scans. Dx = diagnosis; Or = organ; Cy = cyst; Hg = homogeneous; Ne = necrosis; Ma = margins; In = infiltrates in adjacent organs; Mi = extension across midline; En = vascular encasement; Th = tumor thrombosis; LM = liver metastasis; BM = bone marrow metastasis; LN = lymph node.

Standard of Reference

To validate the imaging findings, our standard of reference was surgical notes, histopathologic reports, and at least 12 mo of imaging follow-up.

Image Analysis and Statistics

Three radiologists with 3, 5, and 6 y of experience independently analyzed the MR images without knowledge of the histopathologic results, disease history, or other imaging findings. The unenhanced and enhanced images were evaluated at least 2 wk apart to minimize recall bias. There were 14 diagnostic criteria: image quality on a 4-point scale; organ of origin (primary lesion); tumor solid, cystic, or both; tumor homogeneous or inhomogeneous; tumor margins well-defined or ill-defined; presence or absence of necrosis, infiltration of adjacent organs, extension across the midline, encasement of vessels, tumor thrombosis, solid-organ metastases, bone marrow metastases, and lymph node metastasis; and final diagnosis. Table 2 details those diagnostic criteria that pertain to morphology, extent, and metastases. In the event of multiple primary or metastatic lesions, the interpreters were asked to give a single overall score for the largest lesion in each target organ. Accuracy was calculated on a per-patient basis at each time point: accuracy for 1 subject at 1 time point was scored as 3/3 if all 3 interpreters agreed with the reference, as 2/3 if 2 interpreters agreed with the reference, as 1/3 if 1 interpreter agreed with the reference, and as 0 if none agreed with the reference. Diagnostic accuracy was calculated for every parameter and was compared between the unenhanced and enhanced pairs using bias-corrected and accelerated bootstrap confidence intervals.

For the subgroup of 36 patients with ^{18}F-FDG PET/MR scans, a board-certified pediatric radiologist and a nuclear medicine physician (both with 5 y of experience) compared the unenhanced with the enhanced ^{18}F-FDG PET/MR images regarding the 14 criteria, and diagnostic accuracy was calculated.

In addition, the interpreters evaluated the concordance of ^{18}F-FDG avidity and gadolinium chelate enhancement by consensus on a lesion-by-lesion and patient-by-patient basis. The results were collected in a 2×2 table and compared using the McNemar test. Significant differences were assumed for a P value of less than 0.05.

RESULTS

Comparison of Unenhanced and Enhanced MR Images

Image quality was rated as good to excellent for both unenhanced and enhanced MR images. Unenhanced images received an average score of 3.59 ($\pm$0.63), and enhanced images, 3.63 ($\pm$0.62); these data did not significantly differ ($P > 0.05$).

TABLE 3
Accuracy of 13 Diagnostic Criteria in All 119 Patients

Category	Accuracy before enhancement	Accuracy after enhancement	Difference
Diagnosis	0.678 (0.608–0.737)	0.653 (0.577–0.720)	0.025 (−0.034–0.076)
Organ/location	0.924 (0.880–0.952)	0.899 (0.849–0.930)	0.025 (−0.011–0.062)
Cyst	0.874 (0.815–0.916)	0.826 (0.765–0.871)	0.048 (0.000–0.095)
Homogeneity	0.818 (0.756–0.863)	0.776 (0.711–0.829)	0.042 (−0.020–0.092)
Necrosis	0.664 (0.602–0.717)	0.672 (0.608–0.728)	−0.008 (−0.076–0.050)
Definition of margins	0.725 (0.658–0.783)	0.742 (0.675–0.798)	−0.017 (−0.076–0.036)
Infiltration	0.765 (0.695–0.821)	0.751 (0.683–0.807)	0.014 (−0.039–0.062)
Crossing of midline	0.866 (0.804–0.905)	0.824 (0.756–0.868)	0.042 (0.000–0.087)
Vessel encasement	0.885 (0.835–0.916)	0.826 (0.768–0.868)	0.059 (0.008–0.104)
Thrombosis	0.958 (0.916–0.978)	0.919 (0.866–0.947)	0.039 (0.008–0.073)
Liver metastasis	0.846 (0.793–0.885)	0.857 (0.801–0.896	−0.011 (−0.053–0.025)
Bone marrow metastasis	0.941 (0.890–0.969)	0.91 (0.854–0.944)	0.031 (0.000–0.064)
Lymph node metastasis	0.849 (0.787–0.891)	0.849 (0.784–0.894)	0 (−0.048–0.042)

Data represent relative agreement with standard of reference (1.00 = 100%). Data in brackets are 95% confidence intervals. Differences from the confidence interval not straddling zero were considered significant.

TABLE 4
Accuracy of 13 Diagnostic Criteria in the 36 Patients with ^{18}F-FDG PET/MR Scans

Category	Accuracy before enhancement	Accuracy after enhancement	Difference
Diagnosis	0.667 (0.519–0.778)	0.611 (0.454–0.731)	0.056 (−0.074–0.157)
Organ/location	0.926 (0.833–0.963)	0.87 (0.741–0.935)	0.056 (−0.028–0.148)
Cyst	0.843 (0.694–0.778)	0.75 (0.602–0.852)	0.093 (−0.019–0.204)
Homogeneity	0.667 (0.528–0.778)	0.685 (0.546–0.796)	−0.019 (−0.167–0.093)
Necrosis	0.556 (0.426–0.667)	0.565 (0.417–0.676)	−0.009 (−0.139–0.139)
Definition of margins	0.713 (0.574–0.806)	0.667 (0.519–0.778)	0.046 (−0.065–0.148)
Infiltration	0.63 (0.472–0.472)	0.657 (0.519–0.759)	−0.028 (−0.148–0.083)
Crossing of midline	0.852 (0.750–0.907)	0.833 (0.685–0.907)	0.019 (−0.065–0.111)
Vessel encasement	0.843 (0.728–0.907)	0.787 (0.648–0.870)	0.056 (−0.056–0.157)
Thrombosis	0.898 (0.787–0.954)	0.861 (0.722–0.935)	0.037 (−0.046–0.120)
Liver metastasis	0.852 (0.769–0.898)	0.917 (0.796–0.963)	−0.065 (−0.148–0.019)
Bone marrow metastasis	0.852 (0.704–0.926)	0.806 (0.648–0.898)	0.046 (−0.028–0.130)
Lymph node metastasis	0.843 (0.694–0.926)	0.824 (0.676–0.917)	0.019 (−0.120–0.139)

Data represent relative agreement with standard of reference (1.00 = 100%). Data in brackets are 95% confidence intervals. Differences from the confidence interval not straddling zero were considered significant.

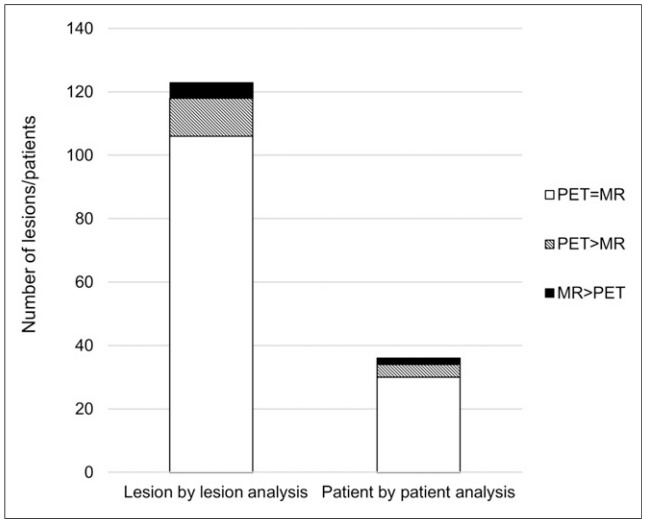

FIGURE 2. Concordance between ^{18}F-FDG PET avidity and gadolinium chelate enhancement. (Left) Lesion-by-lesion analysis of 123 tumors in subgroup of 36 patients with ^{18}F-FDG PET/MR scans. PET = MR, 106/123; PET > MR, 12/123; MR > PET 5/123. (Right) Patient-by-patient analysis in same subgroup. PET = MR, 30/36; PET > MR, 4/36; MR > PET, 2/36.

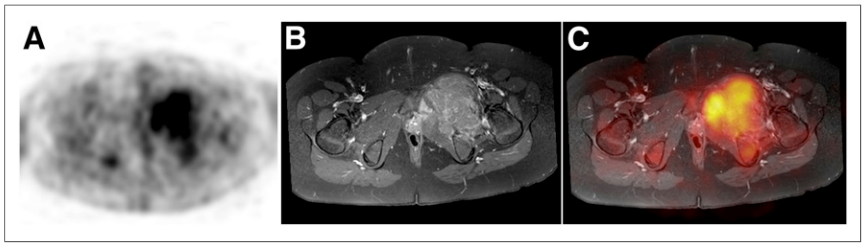

FIGURE 3. Concordance between ^{18}F-FDG PET avidity and gadolinium chelate enhancement (arrows) at initial staging for 11-y-old boy with Ewing sarcoma of left pelvis. (A) ^{18}F-FDG PET image. (B) Enhanced MR image. (C) Enhanced ^{18}F-FDG PET/MR image.

Figure 1A shows the mean data of the interpreters for 13 diagnostic criteria. The accuracies of the diagnostic criteria, calculated as relative agreement with the standard of reference, are depicted in Table 3. There was no significant difference between the unenhanced and enhanced images in the accuracy of any diagnostic criterion. Liver lesions were correctly detected on unenhanced images in 84.6% of cases and on enhanced images in 85.7% of cases, bone marrow lesions in 94.1% compared with 91%, and lymph node lesions in 84.9% compared with 84.9%.

Comparison of Unenhanced and Enhanced ^{18}F-FDG PET/MR Images

Image quality was rated as good to excellent for both the unenhanced and the enhanced ^{18}F-FDG PET/MR images. The unenhanced images received an average score of 3.6 (±0.43), and the enhanced images received an average score of 3.7 (±0.31); these data did not significantly differ ($P > 0.05$). Likewise, accuracy for the 13 diagnostic criteria did not significantly differ between the unenhanced and enhanced images ($P < 0.05$) (Table 4; Fig. 1B).

Lesion-by-lesion analysis revealed concordance between ^{18}F-FDG avidity and gadolinium chelate enhancement for 106 of the 123 tumors (86%) and discordance for 17 (14%). When evaluated on a patient-by-patient basis, 30 patients demonstrated concordance between ^{18}F-FDG avidity and gadolinium chelate enhancement for all tumors and 6 demonstrated discordance for at least 1 tumor. These differences were not significant ($P > 0.05$) (Figs. 2–4).

Regarding the discordances, there were 3 cases of malignant sarcoma in which the area of gadolinium chelate enhancement surrounded but was larger than the area of ^{18}F-FDG avidity. In 2 cases of calcified metastases of a malignant germ cell tumor and 1 case of post–renal transplantation

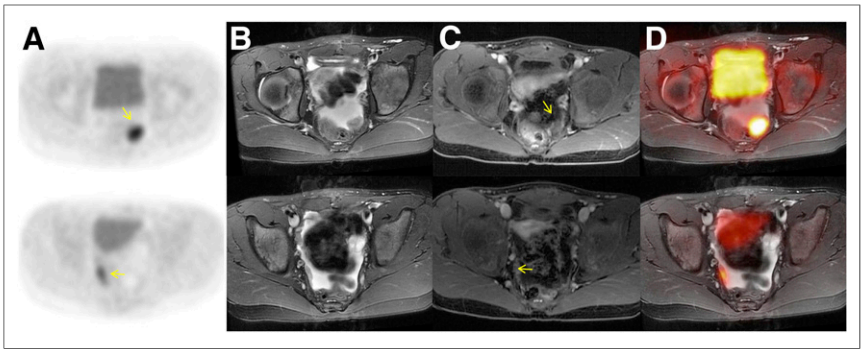

FIGURE 4. Concordance between ^{18}F-FDG PET avidity and gadolinium chelate enhancement in 10-y-old girl after resection of immature teratoma. (A) ^{18}F-FDG PET image demonstrates 2 foci of marked glucose hypermetabolism in left and right lower pelvis (arrows). (B) T2-weighted MR image shows that these foci correspond to small soft-tissue nodules outlined by pelvic fluid. (C) T1-weighted MR image after contrast administration shows enhancement of these nodules (arrows). (D) T2-weighted PET/MR image shows the nodules amid pelvic fluid.

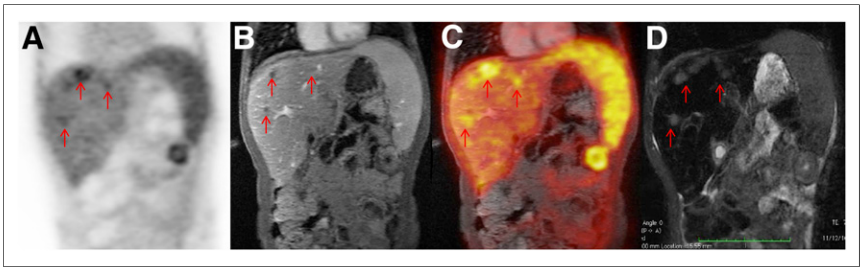

FIGURE 5. Discordance between ^{18}F-FDG avidity and gadolinium chelate enhancement in 10-y-old boy after treatment for desmoplastic small round cell tumor metastasis. (A) ^{18}F-FDG PET image. (B) Enhanced T1-weighted MR image. (C) Enhanced T1-weighted ^{18}F-FDG PET/MR image. (D) T2-weighted MR image. Hepatic metastases are ^{18}F-FDG–avid, but in this case there are multiple hepatic metastases that apparently do not enhance.

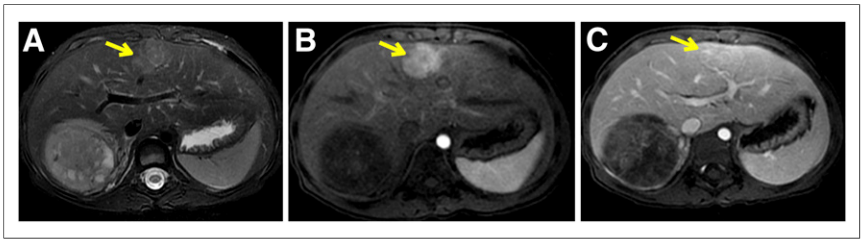

FIGURE 6. Comparison of unenhanced and enhanced MR images in patient with Wilms tumor of right kidney. (A) Before contrast administration, T2-weighted bright lesion (arrow) in right lobe of liver is suggestive of metastasis. (B) After contrast administration, early image shows arterial enhancement. (C) On delayed image, persistence of enhancement in central scar is consistent with focal nodular hyperplasia.

lymphoproliferative disorder, there was marked ^{18}F-FDG avidity but little or no gadolinium chelate enhancement. In 6 cases, hepatic metastases of a germ cell tumor appeared hypointense during all phases after gadolinium chelate injection yet showed marked ^{18}F-FDG avidity (Fig. 5); on CT images, these lesions showed calcification. Only 1 lesion was false-negative on ^{18}F-FDG PET, in a patient with lymphoma: the lesion, which corresponded to epidural disease, was clearly apparent on enhanced MRI but was not detected on ^{18}F-FDG PET, possibly because the PET images were of lower resolution than the MR images.

DISCUSSION

Our data showed no significant difference in diagnostic accuracy between gadolinium chelate–enhanced and unenhanced MR images or between gadolinium chelate–enhanced and unenhanced ^{18}F-FDG PET/MR images for staging of pediatric tumors. There was a high degree of concordance between ^{18}F-FDG avidity and gadolinium chelate enhancement. We conclude that gadolinium chelate contrast administration may not be necessary for integrated ^{18}F-FDG PET/MRI.

Several investigators have reported that T1-weighted fat-suppressed contrast-enhanced MR sequences are superior to unenhanced sequences for tumor diagnosis—for example, in the spine (*14*), the kidney (*15*), and the head and neck (*16*). Contrast enhancement improved lesion detection, tissue characterization, and determination of tumor extent. However, advances in MR technology and improvements in soft-tissue contrast and anatomic resolution on high-field MR scanners give rise to the question of whether administration of contrast agent is always needed. Tokuda et al., in comparing fast short-τ inversion recovery MR sequences with contrast-enhanced sequences, found comparable results for differentiation of benign from malignant tumors in soft-tissue masses (*17*) and even better results for differentiation of benign from malignant bone tumors (*18*), suggesting that contrast enhancement is not always needed. In addition, diffusion-weighted sequences provide information on whether tumors are solid or have cystic or necrotic areas—information that previously was accessible only through contrast-enhanced sequences (*19*). Diffusion-weighted imaging was also found to be superior for detecting small peritoneal and serosal metastases that were difficult to detect on gadolinium chelate–enhanced images (*20*), in addition to showing contrast between tumors and bowel contents better than enhanced images could (*20*) and providing results equivalent to ^{18}F-FDG PET/CT in patients with lymphoma (*11*). In accordance with these studies, we found diagnostic accuracy for local tumor staging to be similar between T2- or diffusion-weighted MR images and gadolinium chelate–enhanced MR images.

Our study and others have found that diffusion-weighted and T2-weighted MRI have a limited ability to characterize focal liver lesions (Fig. 6) (*21*). We therefore suggest that the administration of gadolinium chelates may be necessary only if equivocal liver lesions are identified on unenhanced sequences. This could be especially useful in, for example, differentiation between focal nodular hyperplasia/adenomas and hepatoblastomas/metastases,

which often requires a 2-step approach with a more specific contrast agent such as gadolinium-ethoxybenzyl-diethylenetriamine pentaacetic acid (*22,23*). In such cases, obtaining unenhanced sequences might be advantageous by allowing the examiner to add more specific contrast agents in the same session.

Our data also showed that integrated ^{18}F-FDG PET/MRI does not require gadolinium chelate–enhanced sequences for local tumor staging. Considering the risk of nephrogenic sclerosis (*24,25*) and the recent reports of gadolinium chelate deposition in the brain (*26,27*), as well as the additional cost and time for contrast-enhanced sequences, there would be a major benefit to eliminating gadolinium chelate administration and streamlining pediatric PET/MR studies. Growing cancers are characterized by angiogenesis (*28*) and glucose metabolism (*29*). Previous studies have shown that gadolinium chelate–enhanced sequences can detect vascularized tumor tissue (*30*). However, Kuhn et al. described an improved morphologic characterization of PET-positive primary tumors on T2-weighted PET/MRI compared with contrast-enhanced PET/CT (*31*). Zasadny and colleges reported a strong correlation between ^{18}F-FDG avidity and tumor blood flow in women with untreated breast cancers (*32*). Similarly, Armbruster et al. found a positive correlation between the arterial flow fraction and SUV of liver metastases of neuroendocrine tumors, suggesting a link between arterial tumor perfusion and metabolic activity (*33*). However, tumor blood flow is assessed on a first-pass scan 2 min after contrast administration whereas tumor ^{18}F-FDG metabolism is assessed on scans obtained 30–60 min after contrast administration (*34*). In our study, gadolinium chelate enhancement and ^{18}F-FDG avidity were mismatched in 17 of 123 tumors (Fig. 6). Two of these tumors were sarcomas, which have a known marked heterogeneity (*35*). Other mismatches included ^{18}F-FDG–positive tumors that did not show gadolinium chelate enhancement because of calcification (germ cell tumors) or relatively low blood volume (post–renal transplantation lymphoproliferative disorder) and ^{18}F-FDG–negative tumors that were false-negative because of low PET resolution (lymphoma).

We acknowledge several limitations to our study. Our pediatric population that underwent fused serial ^{18}F-FDG PET/MRI was relatively small, at 36 patients, although to our knowledge this is the largest such population described to date. The heterogeneity of tumor types in our study reflects the typical pediatric imaging practice at our institution, yet because of this variety any conclusions may be overgeneralized. We did not obtain simultaneous ^{18}F-FDG PET/MR images but rather fused serial MR and ^{18}F-FDG PET images, for which image registration is important. We used the well-established Osirix software, which enables registration of MR images to within 500 μm. In a few patients, we included markers on the skin to facilitate this process and found excellent coregistration with our approach. Moreover, even simultaneous PET/MRI still has some limitations in comparison with PET/CT (*36*). Not all of the MR studies used for fused PET/MR images were conducted on the 3-T system. However, there is currently no evidence suggesting that standard sequences on 3-T and 1.5-T systems differ in diagnostic accuracy for pediatric tumors (*37*). Our study included only a single malignant lesion smaller than 1 cm, which is below the anatomic resolution of PET. Our results might have been less favorable for ^{18}F-FDG PET if more subcentimeter-sized lesions had been included. However, tumors in pediatric patients are typically large, with subcentimeter-sized lesions being rare in clinical practice.

CONCLUSION

^{18}F-FDG PET images of pediatric tumors of the abdomen or pelvis can be integrated with either unenhanced T2-weighted MR images or contrast-enhanced T1-weighted MR images. ^{18}F-FDG avidity and gadolinium chelate enhancement show a high degree of concordance in these tumors. If gadolinium chelate enhancement of MR images does not provide additional information compared with ^{18}F-FDG PET images, MR images for local staging can be streamlined and gadolinium chelates replaced by more specific MR contrast agents.

DISCLOSURE

The costs of publication of this article were defrayed in part by the payment of page charges. Therefore, and solely to indicate this fact, this article is hereby marked "advertisement" in accordance with 18 USC section 1734. Financial support was provided by the Child Health Research Institute of Stanford University and the National Institute of Child Health and Development (R01 HD081123-01A1). No other potential conflict of interest relevant to this article was reported.

ACKNOWLEDGMENTS

We thank Dr. Ying Chen for providing valuable input on statistical analysis; Drs. David Weinreb and Bo Yoon Ha for helping with image analysis; and Prof. Sandy Napel for providing valuable input on image processing.

REFERENCES

1. Ley S, Ley-Zaporozhan J, Gunther P, Deubzer HE, Witt O, Schenk JP. Neuroblastoma imaging. *Rofo.* 2011;183:217–225.
2. Siegel MJ, Chung EM. Wilms' tumor and other pediatric renal masses. *Magn Reson Imaging Clin N Am.* 2008;16:479–497.
3. Kremer N, Walther AE, Tiao GM. Management of hepatoblastoma: an update. *Curr Opin Pediatr.* 2014;26:362–369.
4. Lee JM, Yoon JH, Joo I, Woo HS. Recent advances in CT and MR imaging for evaluation of hepatocellular carcinoma. *Liver Cancer.* 2012;1:22–40.
5. Brisse H, Ollivier L, Edeline V, et al. Imaging of malignant tumours of the long bones in children: monitoring response to neoadjuvant chemotherapy and preoperative assessment. *Pediatr Radiol.* 2004;34:595–605.
6. Cha S. Neuroimaging in neuro-oncology. *Neurotherapeutics.* 2009;6:465–477.
7. Iagaru A, Quon A, McDougall IR, Gambhir SS. F-18 FDG PET/CT evaluation of osseous and soft tissue sarcomas. *Clin Nucl Med.* 2006;31:754–760.
8. Kwee TC, van Ufford HM, Beek FJ, et al. Whole-body MRI, including diffusion-weighted imaging, for the initial staging of malignant lymphoma: comparison to computed tomography. *Invest Radiol.* 2009;44:683–690.
9. Catalano OA, Rosen BR, Sahani DV, et al. Clinical impact of PET/MR imaging in patients with cancer undergoing same-day PET/CT: initial experience in 134 patients—a hypothesis-generating exploratory study. *Radiology.* 2013;269:857–869.
10. Hirsch FW, Sattler B, Sorge I, et al. PET/MR in children. Initial clinical experience in paediatric oncology using an integrated PET/MR scanner. *Pediatr Radiol.* 2013;43:860–875.
11. Klenk C, Gawande R, Uslu L, et al. Ionising radiation-free whole-body MRI versus ^{18}F-fluorodeoxyglucose PET/CT scans for children and young adults with cancer: a prospective, non-randomised, single-centre study. *Lancet Oncol.* 2014;15:275–285.
12. Daldrup-Link HE, Golovko D, Ruffell B, et al. MRI of tumor-associated macrophages with clinically applicable iron oxide nanoparticles. *Clin Cancer Res.* 2011;17:5695–5704.
13. Rosset A, Spadola L, Ratib O. OsiriX: an open-source software for navigating in multidimensional DICOM images. *J Digit Imaging.* 2004;17:205–216.
14. Tien RD, Olson EM, Zee CS. Diseases of the lumbar spine: findings on fat-suppression MR imaging. *AJR.* 1992;159:95–99.

15. Semelka RC, Hricak H, Stevens SK, Finegold R, Tomei E, Carroll PR. Combined gadolinium-enhanced and fat-saturation MR imaging of renal masses. *Radiology.* 1991;178:803–809.
16. Barakos JA, Dillon WP, Chew WM. Orbit, skull base, and pharynx: contrast-enhanced fat suppression MR imaging. *Radiology.* 1991;179:191–198.
17. Tokuda O, Harada Y, Matsunaga N. MRI of soft-tissue tumors: fast STIR sequence as substitute for T1-weighted fat-suppressed contrast-enhanced spin-echo sequence. *AJR.* 2009;193:1607–1614.
18. Tokuda O, Hayashi N, Matsunaga N. MRI of bone tumors: fast STIR imaging as a substitute for T1-weighted contrast-enhanced fat-suppressed spin-echo imaging. *J Magn Reson Imaging.* 2004;19:475–481.
19. Eberhardt SC, Johnson JA, Parsons RB. Oncology imaging in the abdomen and pelvis: where cancer hides. *Abdom Imaging.* 2013;38:647–671.
20. Low RN, Gurney J. Diffusion-weighted MRI (DWI) in the oncology patient: value of breathhold DWI compared to unenhanced and gadolinium-enhanced MRI. *J Magn Reson Imaging.* 2007;25:848–858.
21. Park MS, Kim S, Patel J, et al. Hepatocellular carcinoma: detection with diffusion-weighted versus contrast-enhanced magnetic resonance imaging in pretransplant patients. *Hepatology.* 2012;56:140–148.
22. Van Beers BE, Pastor CM, Hussain HK. Primovist, Eovist: what to expect? *J Hepatol.* 2012;57:421–429.
23. Jhaveri K, Cleary S, Audet P, et al. Consensus statements from a multidisciplinary expert panel on the utilization and application of a liver-specific MRI contrast agent (gadoxetic acid). *AJR.* 2015;204:498–509.
24. Weinreb JC, Kuo PH. Nephrogenic systemic fibrosis. *Magn Reson Imaging Clin N Am.* 2009;17:159–167.
25. Weller A, Barber JL, Olsen OE. Gadolinium and nephrogenic systemic fibrosis: an update. *Pediatr Nephrol.* 2014;29:1927–1937.
26. Karabulut N. Gadolinium deposition in the brain: another concern regarding gadolinium-based contrast agents. *Diagn Interv Radiol.* 2015;21:269–270.
27. McDonald RJ, McDonald JS, Kallmes DF, et al. Intracranial gadolinium deposition after contrast-enhanced MR imaging. *Radiology.* 2015;275:772–782.
28. Folkman J. Seminars in medicine of the Beth Israel Hospital, Boston: clinical applications of research on angiogenesis. *N Engl J Med.* 1995;333:1757–1763.
29. Mérida I, Avila-Flores A. Tumor metabolism: new opportunities for cancer therapy. *Clin Transl Oncol.* 2006;8:711–716.
30. Tuncbilek N, Kaplan M, Altaner S, et al. Value of dynamic contrast-enhanced MRI and correlation with tumor angiogenesis in bladder cancer. *AJR.* 2009;192:949–955.
31. Kuhn FP, Hullner M, Mader CE, et al. Contrast-enhanced PET/MR imaging versus contrast-enhanced PET/CT in head and neck cancer: how much MR information is needed? *J Nucl Med.* 2014;55:551–558.
32. Zasadny KR, Tatsumi M, Wahl RL. FDG metabolism and uptake versus blood flow in women with untreated primary breast cancers. *Eur J Nucl Med Mol Imaging.* 2003;30:274–280.
33. Armbruster M, Sourbron S, Haug A, et al. Evaluation of neuroendocrine liver metastases: a comparison of dynamic contrast-enhanced magnetic resonance imaging and positron emission tomography/computed tomography. *Invest Radiol.* 2014;49:7–14.
34. Mullani NA, Herbst RS, O'Neil RG, Gould KL, Barron BJ, Abbruzzese JL. Tumor blood flow measured by PET dynamic imaging of first-pass ^{18}F-FDG uptake: a comparison with ^{15}O-labeled water-measured blood flow. *J Nucl Med.* 2008;49:517–523.
35. Bestic JM, Peterson JJ, Bancroft LW. Pediatric FDG PET/CT: physiologic uptake, normal variants, and benign conditions. *Radiographics.* 2009;29:1487–1500.
36. Bezrukov I, Schmidt H, Gatidis S, et al. Quantitative evaluation of segmentation- and atlas-based attenuation correction for PET/MR on pediatric patients. *J Nucl Med.* 2015;56:1067–1074.
37. Wardlaw JM, Brindle W, Casado AM, et al. A systematic review of the utility of 1.5 versus 3 Tesla magnetic resonance brain imaging in clinical practice and research. *Eur Radiol.* 2012;22:2295–2303.